EUROPEAN FUSION DEVELOPMENT AGREEMENT

EFDA–JET–PR(00)10

H Chen et al

Impurity Transport with Strong and Weak Internal Thermal Barriers in JET Optimised Shear Plasma

Impurity Transport with Strong and Weak Internal Thermal Barriers in JET Optimised Shear Plasma

H Chen[1*], M G Haines[1], N C Hawkes, L C Ingesson, N J Peacock[1].

EURATOM/UKAEA Fusion Association, Culham Science Centre,
Abingdon, Oxfordshire, OX14 3DB, UK.
[1]Imperial College, The Blackett Laboratory, London, SW7 2BZ, UK.
[1*]Present Address: Lawrence Livermore National Laboratory, Livermore, CA 94551, USA.

ABSTRACT

Results of particle transport analysis are presented for both low and high-charge impurity species in Joint European Torus (JET) Optimised Shear (OS) plasmas. The content of impurities in the plasma centre is sensitive to the strength of the internal transport barrier. In a strong transport barrier plasma, the diffusion coefficient in the centre is about one order of magnitude lower than than in plasmas with weak transport barriers. Impurity transport is close to the neoclassical transport prediction in the centre of the plasma whereas it is much higher than neoclassical theory in the plasma edge. A convection term in the vicinity of the transport barrier was required in order to account for the measurements. These data support theories of turbulence suppression by the $E \times B$ shearing rate.

1. INTRODUCTION

Reversed magnetic shear is considered a good candidate for improving the tokamak concept as a fusion reactor could operate with low plasma current, and this would lead to a steady-state operational configuration [1]. Experiments on manipulating the magnetic shear have been performed in tokamak devices such as on TFTR [1], DIIID [2], JET [3] and JT-60U [4]. An Internal Transport Barrier (ITB) appears to be an outstanding common feature among this type of high confinement experiment in tokamaks. The ITB appears as a steep gradient in the pressure profile, typically locates around half the minor radius, and ITB is believed to be the result of reduced transport of particles, momentum, and energy [5]. This type of plasma confinement mode has attracted a great deal of research effort.

Understanding the behaviour of impurities remains one of the main concerns in the magnetic shear experiment for well-known reasons: impurities can cause a severe radiated power loss and fuel dilution and they also affect plasma stability. Testing the available theoretical predictions still remains one of the main tasks for the experimental investigation of impurity transport.

Since the turbulence-induced transport may be reduced in the ITB region of plasmas, this type of high confinement provides a good chance to experimentally verify the neoclassical transport theory [6]. For instance, Wade *et al.* [7] reported evidence of neoclassical impurity transport observed on light impurity ions, such as carbon and neon, in DIII-D during high confinement experiments. In other confinement conditions such as High (H-mode) and Low (L-mode) mode confinement plasmas, the radial transport of impurities have been found to be low in the core of the plasma by various investigations. For example, Giannella *et al.* [8] have studied elements including Ni and Fe impurities in the JET L-mode plasmas. It was found that the central diffusion coefficient is 0.2 m^2/s, which is about an order of magnitude lower than the diffusion coefficient in the edge region, but still over an order of magnitude higher than the neoclassical prediction. Supportive results have been reported from studies in Tore Supra [9]. For H-mode plasmas, studies in ASDEX Upgrade [10] show that the impurity transport is less

than 0.06 m^2/s and increase to 2 m^2/s in the edge region. A recent comprehensive review on the ion transport and confinement is given by ITER Physics Expert Groups [11].

In this paper, we present the results of impurity transport studies in JET plasma during Optimised Shear (OS) experiments. We discuss several aspects including deriving the impurity transport in the OS plasma from diagnostics that measure impurity radiation, establishing the correlation between the strength of ITB and the impurity transport, observing the accumulation of impurities in different stages of confinement and studying the Z-dependence of the impurity transport. For these purposes, two impurity species were chosen: intrinsic carbon (Z = 6) and injected nickel (Z = 28) using a well-developed laser injection technique as described by Giannella *et al.* [8]. The impurity experiments and diagnostics are described in Section 2. Section 3 reports the experimental results. The results of impurity transport simulation are presented in Section 4, while theoretical interpretations are discussed in Section 5. A summary is given in Section 6.

2. EXPERIMENTAL CONDITION

JET optimised shear experiments were performed in the single null lower X-point configuration. The plasma current was 3.2 – 3.5 MA and magnetic field 3.4 – 3.6 T. Auxiliary heating included Neutral Beam Injection (NBI) and Ion Cyclotron Resonance Frequency (ICRF) heating with heating powers of up to 20 MW and 10 MW, respectively. The best performance achieved D-D neutron production rates in the range of $5.0\times10^{16}\ s^{-1}$ with electron temperature and densities of 12 keV and $6\times10^{19}\ m^{-3}$ and ion temperatures, measured with fully stripped carbon, of about 26 keV.

Trace impurity was injected by a laser blow-off system [12]. The laser source is provided by a ruby laser. The pulse duration is about 20 ns and the single pulse power is selectable from 3 J to 20 J. The target has a 5 mm coating of impurities on a glass slide, of which a region with diameter 2 — 6 mm is ablated. For nickel the number of the atoms ablated is about a few 10^{18}. The impurity forms a cloud of atoms with an average energy of about 2 eV. The criterion of a "trace" impurity injection is that the change in the main plasma parameters due to the injection is small, non-perturbing. Experimentally, the injected impurity nickel density is found to be of the order of $10^{15}\ m^{-3}$, and its influence on the plasma current and electron density is less than 1%.

The evolution of nickel ions in the main plasma is followed by a 216-Channel Soft X-Ray (SXR) multi-camera system [13]. The camera has a 250 mm beryllium window to isolate it from the main vacuum, which limits the lower photon energy to about 2 keV. Time dependent emission profiles of nickel ions are derived from the local Soft X-Ray emission reconstructed by a tomographic technique which has been described in [14]. The SXR system in JET provides a powerful diagnostic tool for measuring the nickel ion emission because nickel is a good radiator

in the Soft X-Ray region. Impurity injection experiments were in co-ordinates with the fast data acquisition window, and this ensured that the injection period was recorded with a 250 kHz data acquisition frequency for up to a second [15]. Outside this time window, emission data was collected at a frequency of 5 kHz. In addition, the total power radiated is measured with multi-chord bolometric diagnostics [16] and the line emission of the ions monitored with a SPRED VUV spectrometer [17] and crystal Soft X-Ray spectrometers [18]. The density and temperature profiles of intrinsic carbon are obtained from the measurements of the charge-exchange diagnostic system [19].

3. EXPERIMENTAL RESULTS

3.1. General description of intrinsic impurity content in OS plasmas

The variation of impurity content in a typical JET OS plasma is shown in Figure 1. During the OS confinement, the Z_{eff} does not change much (Z_{eff}~2,). The carbon concentration varies slowly with time and increases slightly in the centre of the plasma. A slow accumulation of impurities has been observed in the centre of the OS plasmas with an L-mode edge. Similar observations have also been reported in DIIID [20] and TFTR [21]. In some of the OS plasmas, hollow carbon density profiles have been observed while the electron density is centrally peaked. A drastic change in various plasma parameters occurs when the plasma transits into an ELM-free H-mode. The electron density increases and its profile becomes broader. There is an abrupt increase of ion temperature at the edge. The carbon density increases everywhere in the plasma to about 2 times higher compared to its density in OS confinement, particularly in the centre of the plasma, where the concentration increases from about 1% to 3%.

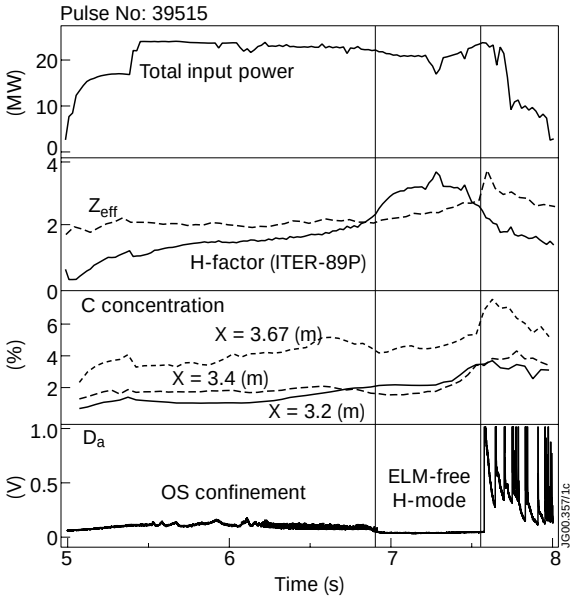

Figure 1: The variations of impurity content in an OS discharge. The H-factor using scaling ITER-89P. X is the major radius, and the magnetic axis is at about X = 3 m.

When ELMs appear following the ELM-free phase, the ion temperature drops everywhere in the plasma, but the electron density increases particularly in the edge region, and its profile becomes flat. Z_{eff} increases to about 2.5, whilst the carbon density and concentration show a large increase at the edge (perhaps due to the sudden increase of the impurity source from sputtering). The relatively long time-scales for the penetration of impurities (i.e. slow transport process) result in a small increase in the central region.

3.2. Dependence of impurity transport on the strength of the internal transport barrier

The gradients in the ion temperature profiles in OS discharges, as shown in Figure 2(a) and 2(b), fall into two groups identified with different strength of the ITB (we define $1/L_{Ti} = \nabla T_i / T_i$ as the strength of an ITB). One group has a strong ITB ($1/L_{Ti} \geq 10$ m^{-1}, see Table 1) and the other a weak ITB ($1/L_{Ti} < 10$ m^{-1}). This distinction between the two groups does not show as clearly in the profiles of the electron density and temperature as in the ion temperature profile.

The injected impurity behaviour is very different in the two groups of OS plasmas. With a strong ITB ($1/L_{Ti} >12$), the impurity radiation has features as shown in Figure 2(c), and in the plasmas with weak ITB ($1/L_{Ti} <10$) its radiation shows in Figure 2(d). In both strong and weak ITB plasmas, the rise-time of the line intensities is short (50 ms – 70 ms). In the weak ITB case the rise and decay of the line intensities of the Ni XXV, Ni XXVI and Ni XXVII are all fast (as in discharge 38441). The decay of the line intensity in the weak ITB case shows that there is a similarity in Li-like (Ni XXVI) and He-like (Ni XXVII) nickel ions. The decay time is about 350 ms. In the strong ITB case, however, there are distinct differences in the time history of the line intensities of Ni XXV and the other lines: while the rise times of the three lines are similar, the decay times are very different. The longer decay time of Li-like and He-like ions seems to indicate a good confinement for the ions. This is in stark contrast to the case of a weak ITB plasma where residence time of nickel ions is short. These two types of behaviour are strongly correlated to the strength of the thermal barrier. Table 1 lists discharges that have different ITB strengths.

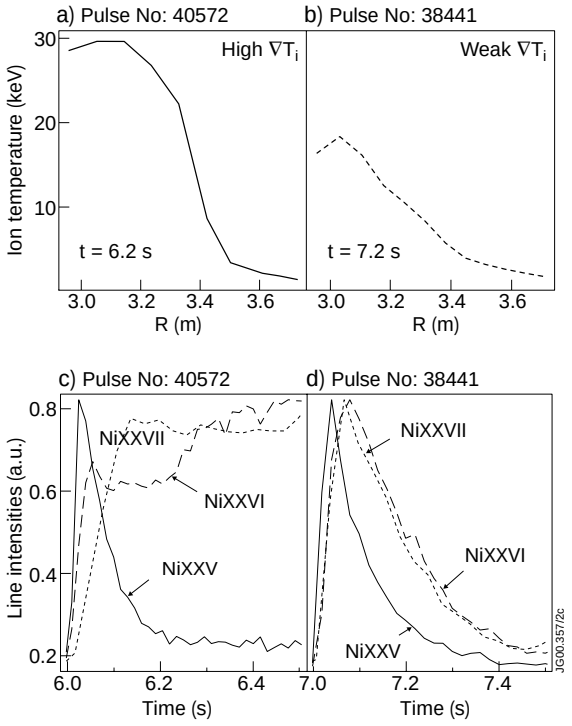

Figure 2: The ion temperature profiles and the time history of Ni VUV line spectra in the OS plasmas with strong ITB (a, c) and weak ITB (b,d).

It is difficult to resolve the detailed composition of the broadband Soft X-Ray radiation in a plasma partly because of unknown impurity populations of each ion species, and also because of the complexity of the radiation channels of each ion species. In order to understand the radiation components recorded with the Soft X-Ray camera, we made an estimate using the same formula as in the code SANCO [22, 23], and the emission coefficients were taken from the database ADAS [24]. We found that over 90% of Ni radiation in the plasma for radii r/a < 0.5 occurs in the Soft X-Ray region, and over 60% of this radiation is from dielectronic recombination and *bremsstrahlung* radiation. The line radiation in the core accounts for about 30% of the total

nickel radiation. For r/a < 0.5, over 60% of the line radiation in the Soft X-Ray region is from the He-like Ni XXVII, and H-like nickel ions has about 30% of the total line radiation. This is consistent with the results from a Soft X-Ray pulse height analyser which has time resolution of about 100 ms. The spectra shows that, after the nickel injection, superimposed on the continuum background, there is a strong energy peak at about 8 keV. This is identified as helium-like Ni XXVII line emission.

TABLE 1

Parameters in some of the OS confinement plasmas:
ITB position, the strength of the ITB and the scale length of the electron density

Pulse No.	ITB (r/a)	$1/L_{ti}(m^{-1})$	$1/Lne(m^{-1})$		Pulse No.	ITB (r/a)	$1/Lti(m^{-1})$	$1/Lne(m^{-1})$
38441	0.55	5.8	3		40550	0.55	20	5
39572	0.50	6.4	4		40551	0.55	22	5
40048	0.50	11	×		40553	0.50	3.8	×
40068	0.55	12	3		40554	0.60	25	5
40069	0.45	5.8	3		40556	0.55	5.4	×
40074	0.45	10	4		40570	0.53	17	3.8
40086	0.50	4	2		40571	0.60	20	3.4
40542	0.60	12.4	5		40572	0.55	23	×

×: a definite number cannot be derived because of the poor quality of the data from that discharge

The Ni XXVII line at about 8 keV is the main contributor to the background subtracted Soft X-Ray signals. Tomographic reconstruction of the background subtracted Soft X-Ray images provides the temporal behaviour of Ni XXVII radiation and therefore helps us to understand the behaviour of the line-integrated Ni XXVII emission shown in Figure 2. The results of the tomographic reconstruction also show the large difference between OS plasmas with weak and strong ITB. Figure 3, in which the background emissivity (taken at 7.011 s, a few milliseconds before the injection) has been subtracted, shows a set of Soft X-Ray tomographic images of Ni injection into a weak ITB plasma. The emission ring is visible at 9 ms after the injection. Within 69 ms after the injection the peak of emission is already in the core of the plasma. This centrally peaked radiation decays immediately, and about 400 ms after the injection, Ni radiation decays to the background level.

In a strong ITB plasma, as shown in Figure 4, the ring-like structure of the Ni emissivity appears at the mid-plasma radii at 65 ms after the injection, which is similar to the observations in the previous case. However, the peak does not move to the plasma centre as in the previous case. On the contrary, it stays at half the plasma radius for over 200 ms. This observation indicates that there is a “barrier” to the influx of particles at the location at the thermal transport barrier,

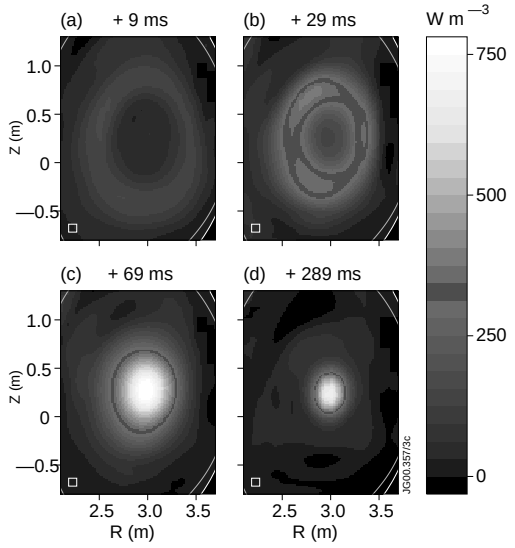

Figure 3: Background-subtracted tomographic images of nickel Soft X-Ray emissivity in a weak ITB OS plasma (38441). The times shown are relative to the nickel injection time. The box in the lower left corner indicates the grid size used in the reconstructions.

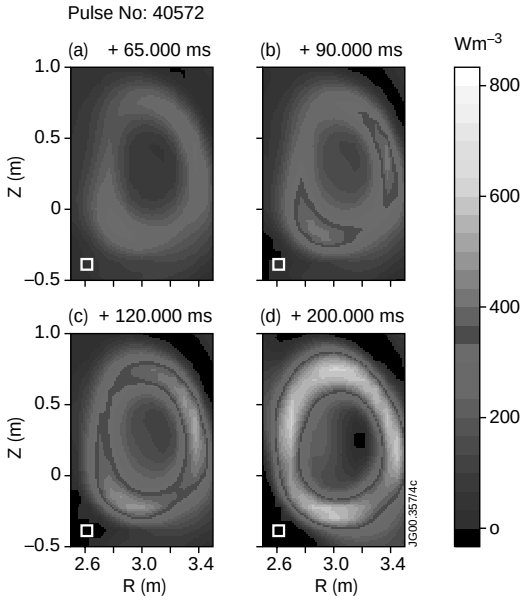

Figure 4: Background-subtracted tomographic images of nickel Soft X-Ray emissivity in a strong ITB plasma (40572). The times shown are relative to the time of nickel injection.

i.e. ion particles cannot get through the barrier region quickly, as they do in the case of a weak ITB plasma. For the time beyond 200 ms after the injection, subtracting x-ray signal of Ni ions from the Soft X-Ray camera data became less satisfactory because of the variations on the plasma conditions from the ones taken as the background.

Carbon is the most abundant intrinsic impurity in JET plasmas. Given the plasma temperature, most carbon in the plasma is fully stripped and its density, temperature and toroidal rotation velocity profiles are measured using charge exchange diagnostics. The evolution of carbon density profiles also differs in the two types of OS plasmas, see Figure 5. The C^{6+} density profile remains hollow in the weak ITB plasma (38441) and slowly evolves towards a less hollow shape; the greatest gradient of C density practically coincides with the location of the ITB. In a strong ITB plasma (40572), the intrinsic C impurity also shows a progressive mild accumulation towards the centre with the C density profile evolving over about one second from a moderately hollow profile to a moderately peaked profile.

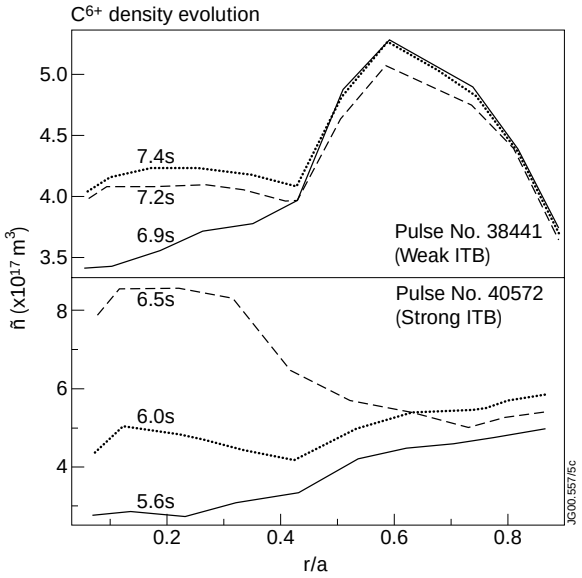

Figure 5: C^{6+} density profile evolution in the OS plasma with weak ITB (upper box) and strong ITB (lower box).

3.3 The effect of edge conditions on the transport in OS plasmas

During the experiments, we found that in the group of strong ITB discharges there are several exceptional discharges in which nickel ions are confined for a shorter time than they are in other cases. The reason is identified as the ELMy plasma boundary in these discharges. The ELMs in these discharges are classified mostly as Type I (giant) ELMs, and the perturbation on electron temperature at the r/a = 0.45 region is up to 6 keV, according to the electron cyclotron emission (ECE) diagnostics. The difference between an ELMy edge compared to an L-mode edge is summarised in Figure 6 (carbon), and Figure 7 (nickel). The lower carbon densities in the edge plasma (r/a > 0.6) lead to a reduction of carbon concentration in the plasma with an ELMy edge. The confinement of nickel ions in the plasma with ELMy edge resembles the case of a weak ITB plasma where the penetration time of the ion and confinement are both short.

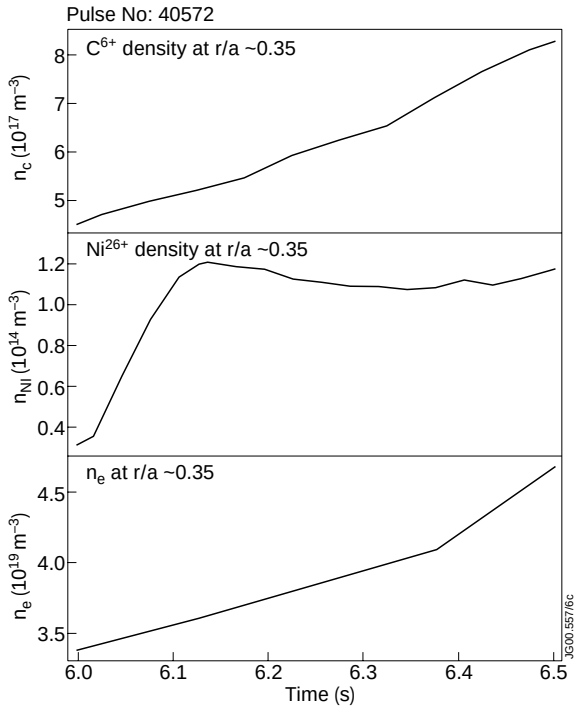

Figure 6: The time evolution of the C^{6+} concentration profile in OS confinement with strong ITB with different edge conditions: with ELMy H-mode (40542) and with L-mode (40572).

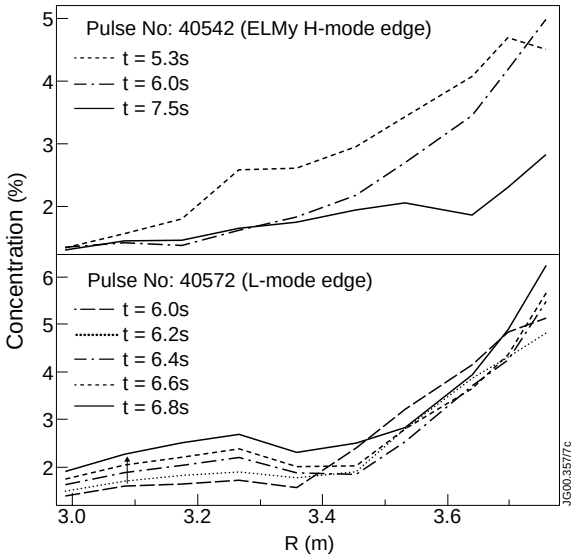

Figure 7: Background-subtracted flux-surface averaged Soft X-Ray emissivity, which is roughly proportional to the Ni^{26+} density in plasmas with strong ITB with with L-mode edge(40572) and ELMy edge (40542).

4. ION TRANSPORT SIMULATION

Impurity transport modelling with experimental data was performed using the 1.5 D transport code SANCO [23]. This code takes the main plasma parameters and actual plasma geometry as input to calculate the non-coronal ionisation balance of impurities. For ion species *I*, the transport model includes diffusive and convective processes and the radial impurity flux is taken to be:

$$\Gamma_I(r)/n_I(r) = -D_I(r)\left(\partial n_I(r)/n_I(r)\right) + V_I(r)$$

In the analysis, the coefficients D and V are assumed to be independent of ion charge and do not vary with time. This model is the simplest description of all the known physical processes, and the neoclassical transport equations can be cast into this parameterised form. To obtain the transport coefficients, we used an interpretative method [8] which is to analyse the functional relation between the normalised impurity fluxes and the gradients of the impurity densities that gives directly the diffusion coefficient and the convection velocity. At each radial position *r* of the source-free region, the local ion flux G_I can be derived from the continuity equation $\partial n_I / \partial t = -(1/r)\partial(r\Gamma_I)/\partial r$. A linear fit to the data points in the transport model (1) gives the transport coefficients *D* and *V.* Then the *D* and *V* coefficients are inserted into the simulation code. By finely adjusting their profiles until a good agreement is achieved between the simulation and the experimental data, a successful model for impurity transport are produced.

To compare the found transport coefficients with predictions from theory, neoclassical transport calculations were performed using the FORCEBAL code [25]. Two impurity species, carbon and nickel, were used in the calculations. Because carbon is the dominant impurity in JET plasma, it is used as the main impurity in the code and nickel as trace impurity. In a similar fashion as the input to the SANCO code, the plasma temperature and density are taken from measurements, and the plasma geometry is from the EFIT [26] plasma equilibrium reconstruction. The radial electric field and toroidal rotation of the plasma are incorporated in the calculations [25], i.e. the measured carbon toroidal rotation is taken as input, and then the radial electric field and the toroidal rotation of other species are determined.

The FORCEBAL code uses the standard treatment in most neoclassical theories [6], that is, the toroidal and parallel flow velocities of impuirties are assumed to be smaller than their thermal velocity. However, a fast toroidal rotation may affect on the poloidal impurity distribution and consequently on the impurity transport. This effect has not yet been implemented in the FORCEBAL code, therefore the code calculation may slightly underestimate the impurity transport coefficients. For the discharges discussed in this paper, the ratio of $v_{tor}/v_{thermal}$ is about 0.8 – 1.4, and the transport enhancement factor on diffusion coefficients are about 1 – 1.5, (ref Section 5.3). For the discharges discussed in this paper, the ratio of and because the measurement of poloidal rotation is not yet available in JET, the neoclassical value is used instead in the calculations.

4.1. Impurity ion transport in weak ITB plasmas

In the plasmas with weak ITBs, injected nickel ions have a rapid inward propagation and a quick decay. The pulses have an L-mode edge, i.e. in D_a signals there are either no ELMs or at most some very small amplitude ELM-like activities.

The interpretative transport analysis using code SANCO indicates that large transport coefficients are required to produce the flux term. As shown in Figure 8, the interpreted transport coefficients

were derived from the Soft X-Ray tomographic reconstruction, Figure 8(a). The impurity density is shown at four time-points from the reconstructed emissivity, see Figure 8(b). Figure 8(c) is the calculated ion flux. The profiles of *D* and *V*, Figure 8(d) and 8(e), were obtained from the fit, and 9(f) shows the correlation of the linear fitting. It is found that nickel propagation appears to be driven by a strong (V = 10–20 m/s) inward convection localised outside the ITB (located approximately at r/a = 0.5). The inward convection velocity decreases towards the centre of the plasma, to a value about 0~2 m/s. The diffusion is larger at r/a ~ 0.8 of the plasma (D ~ 8 m^2/s) than in the core of the plasma (D ~ 0.5 m^2/s).

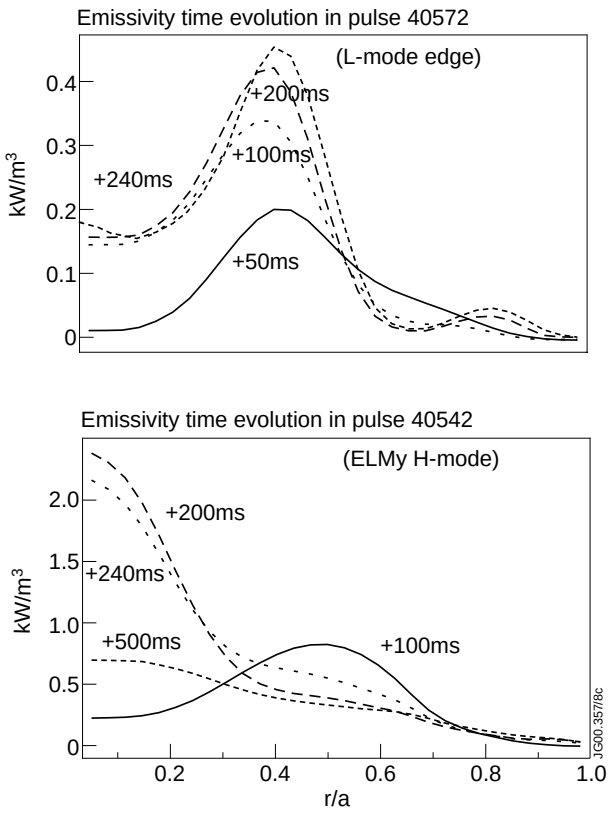

Figure 8: The impurity ion density (b) and flux (c) derived from the flux surface averaged Soft X-Ray emissivities (a) at different times by interpretative simulation for a weak ITB plasma with L-mode edge. The same line style in the three sections indicates the same time (d) and (e) are the transport coefficients derived from the linear relation between the flux term and the ion density gradient (f) the correlation of the fit, where -1 indicates a perfect fit of the data.

With this pair of coefficients, the time evolution of the flux surface averaged Soft X-Ray emission is well reproduced. The line intensities of different ionisation stages were calculated and compared with the measurements by spectrometers. The He-like nickel line was reproduced well with this pair of transport coefficient but difficulties were encountered in the fitting of the Li and Be-like nickel ion line intensities. These ions are mostly populated in the plasma range 0.6 < r/a < 0.9 where the plasma temperature is around 1~5 keV. Using the large transport coefficients obtained from the interpretation of the Soft X-Ray data through to the edge (r/a = 1) resulted in too fast transport of the Li and Be-like ions. Along a central line-of-sight, the line intensity is determined by several factors, such as the electron and ion density, radiation coefficient and radiation energy. Because there is a larger uncertainty in the electron density and temperature measurement in the edge area, in the simulation the edge density and temperature have been varied within a reasonable range to see the effect on the transport simulation.

It is found that by reducing the plasma temperature within the error bars in the measurements, the Be and Li-like ions would shift further in the plasma and stay in the plasma slightly longer, but not longer than a few tens of milliseconds. On the other hand, if one increases the plasma temperature, the Be and Li like ions would be pushed to the edge of the plasma and increase the transport loss of these ions. In a similar fashion, the electron density has been varied. An increase

of electron density could increase the radiation but causes the decrease of impurity density because of increased ionisation rates. We found that adjusting the edge plasma parameters cannot simulate the measured line radiation.

In order to match the decay of Ni XXV line radiation, a small diffusivity ($D \sim 0.2$ m^2/s) has to be used in a narrow region (r/a ~ 0.9) instead. A higher value of D in this area would result in too short a rise and decay time of the line intensity of these ions. Because both D and V terms are included in the flux model, the possibility of using a strong convection velocity only in this region instead of a reduced diffusion coefficient has been tested. It was found difficult to produce a satisfactory fit to the data with a strong convection velocity in the region: a strong convective inward velocity (50 – 100 m/s) combined with a diffusion (~1 m^2/s) tends to result in a fast decay of the Ni^{24+} ions. A region of reduced diffusive transport present at the plasma periphery in the JET L-mode plasmas has previously been reported [27] and [28].

4.2. Ion transport in strong ITB plasmas with L-Mode edge

The plasma density and temperature profiles are more centrally peaked in plasmas with stronger ITBs than in the weak ITB plasmas. The Z_{eff} increases slightly during this confinement, and there is a slight accumulation of light impurities in the core of the plasmas. These OS discharges studied have L-mode edge. The following features are identified during transport simulations.

a) Reduced transport inside the ITB

In plasmas with strong ITBs, it is observed that nickel ions do not penetrate to the centre of the plasma in the time scale of a few hundred milliseconds, although their propagation to the mid-radius is rapid. The “accumulation” position of the nickel ions appears to be in the vicinity of the ITB. To simulate the nickel emission profile, the transport coefficients have to be greatly reduced inside the ITB region. If the nickel diffusion coefficient were chosen higher than 0.1 m^2/s in the centre region in the simulation, nickel ions would be transported into the centre within the time-scale of the experiment. Figure 9 shows the simulated Soft X-Ray emissivity, compared with the flux surface averaged value derived from measurements. The transport coefficients used are shown in Figure 9(c) and 9(d). Inside the ITB, the diffusion coefficient is 0.05 m^2/s, which is comparable to the neocalsscial prediction of 0.03 – 0.06 m^2/s. Outside the ITB, the diffusion coefficient is 0.6 m^2/s that is over an order of magnitude than the neoclassical value that is about 0.02 m^2/s.

The reduction of the diffusion coefficient in the central plasma is not as clear as in the carbon simulation. In the carbon simulation D ~ 0.3 m^2/s was used. C^{6+} density was measured with an error bar of around 20% in the central region. Although one needs a lower diffusion coefficient ($D \leq 0.1$ m^2/s) to simulate the variation of the C^{6+} density, given the data quality, it is difficult to conclude whether the transport of carbon is close to the value of neoclassical transport theory, or whether carbon has a similar shape as nickel.

It has been reported [21] that in TFTR the central ion temperature has a flat profile, which seems to indicate a very large thermal diffusivity in that region. Following this idea, a hypothetical transport model has been tested in the simulation. The proposal is that transport might have been only reduced within the narrow ITB region, instead of having reduced transport over all regions inside the ITB. It is important to find the area of reduced transport since it is believed that in that region the turbulence is suppressed. This hypothesis has been tested in our nickel simulations using the proposed profile of diffusion coefficient, shown in Figure 10.

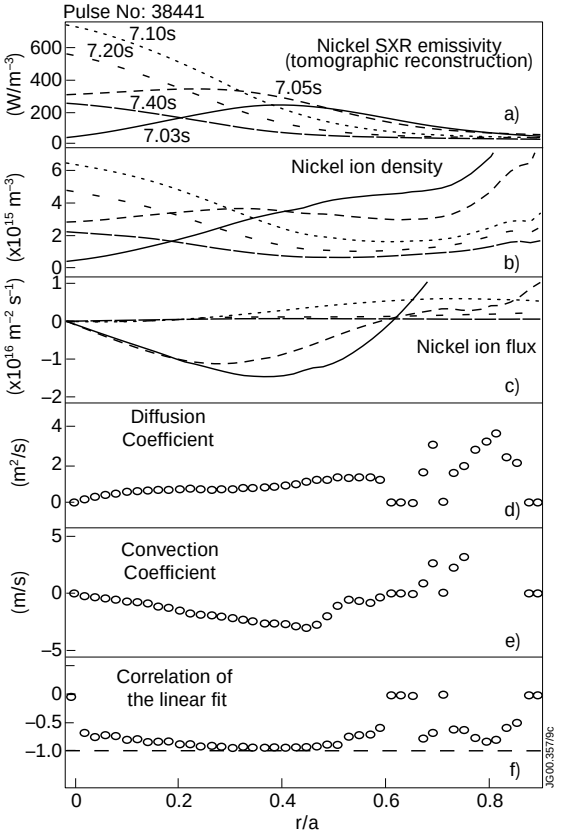

Figure 9: (a) the Soft X-Ray emissivity from the reconstruction from nickel in a strong ITB plasma (40572) with L-mode edge; (b), the simulated emissivity normalised to unity and (c) and (d) are the resulting transport coefficients. The dotted lines in (c) and (d) are the calculated values from the neoclassical theory.

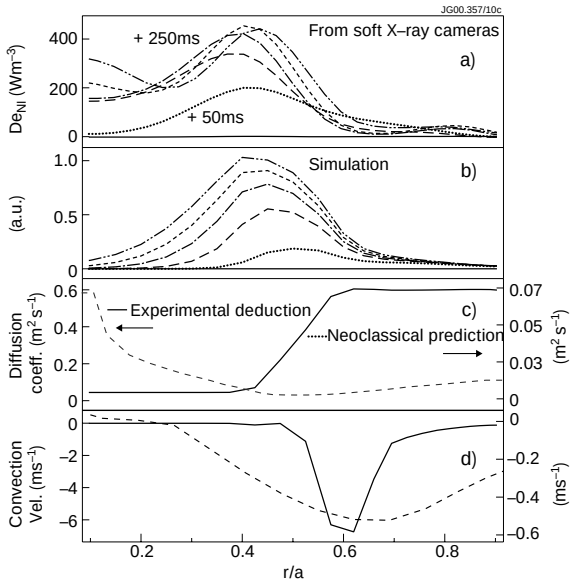

Figure 10: A hypothetical transport coefficient scheme for OS plasmas.

It was found that a high coefficient ($D \sim 1$ m^2/s) in the centre region would result in an inward impurity flux (because of the large impurity density gradient in the ITB region) and the density would fill in the centre region rapidly (in less than 100 ms). However, the experimental data shows that nickel ions do not fill in the region within 200 ms. To overcome this effect, the diffusion in the ITB region would have to be reduced to a value far lower than the neoclassical prediction (for example, $D \sim 0.005$ m^2/s, about an order of magnitude lower than the collisional transport value, D = 0.03 – 0.06 m^2/s). Since collisional transport is generally believed to be the minimum ion transport, the above hypothesis does not offer a plausible description of nickel ion transport.

b) Convection velocity in the ITB region

A strong evidence for an increased convection velocity in the transport barrier comes from the time evolution of density profiles of fully stripped carbon. In plasmas with strong ITBs, the common feature is that the central carbon density increases with time, and a density gradient develops in the region close to the ITB. This indicates an inward flux that comes from an inward convection, as shown in Figure 11.

The inward convection velocity is about 4 m/s in r/a = 0.45, which is around the location of ITB. The inward convection is predicted by neoclassical transport theory and the neoclassical convection velocity has its maximum (0.2 m/s) at around r/a = 0.4 to r/a = 0.5, but this predicted value is still a factor of 20 times lower compared to the simulation.

A further confirmation of the convective nature of the ion transport is given by the temporal evolution of the nickel line radiation. There is a large difference in the time history of the two adjacent ionisation states, Be-like Ni^{24+} and Li-like Ni^{25+} ions, see Figure 2(b). The line intensity from Ni^{24+} peaks at 30 ms after the injection and then rapidly decays, but the Ni^{25+} line intensity does not decay: it grows to a nearly steady value on the same time scale. These two ions have similar ionisation energy (2.297 keV for Ni^{24+} and 2.399 keV for Ni^{25+}) and radiation rate.

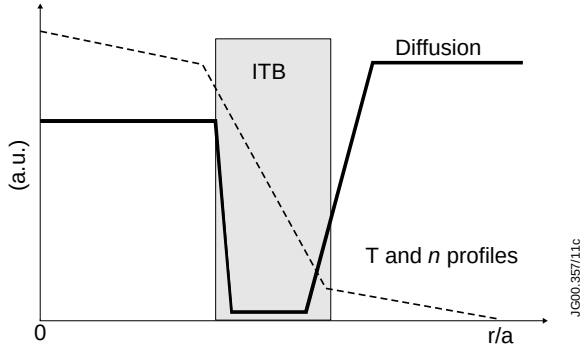

Figure 11: Simulation of C^{6+} profiles in a strong ITB plasma with L-mode edge (40572) and the resulting convection coefficients and its neoclassical prediction. The diffusion coefficient used in the simulation was constant over the radius, $D=0.3\ m^2s^{-1}$.

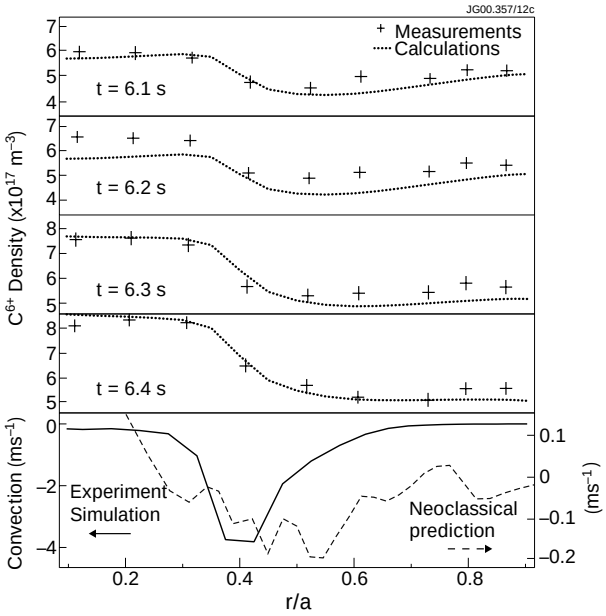

Figure 12: Comparison of Ni diffusion and convection coefficient profiles in a strong ITB plasma (solid line) and weak ITB plasma (dotted lines) with L-mode edge. The thermal ITB is located at radius r/a~0.5.

Therefore the difference in their line intensity behaviour can only be explained by rapid ion transport in this region. Indeed, in the simulation a convection velocity of about 6 –10 m/s is required at the radial position (r/a = 0.5 – 0.7) where the emission shells of these ions are located. It is important to recall that an inward convection velocity is also predicted by neoclassical

theory for Ni ions (Figure 10(d)), although the neoclassical convection value is small: 0.6 m/s at r/a = 0.6, which is an order of magnitude lower than the value used in the simulations.

Figure 12 summarises the transport coefficients for nickel in strong and weak ITB plasmas. In strong ITB plasmas the impurity has a very low diffusion coefficient, a factor of 10 lower than that in the weak ITB plasma. The impurity transport in plasmas with a strong ITB and an ELMy edge seems to be diffusion dominated, with a diffusion coefficient of $D \sim 0.5$ m^2/s in the centre, rising to $D \sim 4$ -5 m^2/s at the edge of the plasma.

4.3. Ion transport in strong ITB with a ELMy H-Mode edge

As indicated in Section 3.4, the plasma edge conditions affect the global ion transport. To make a quantitative assessment, the transport has been analysed for discharge 40542, which has both a strong ITB and an ELMy edge. The measured and simulated flux surface averaged Soft X emissivity profiles and the deduced transport coefficients are shown in Figure 13. The impurity ion transport of the strong ITB plasma with an ELMy edge is similar to that of a weak ITB plasma. The plasma with an ELMy edge has a higher level of the radial transport and that prevents the core accumulation of impurities. Table 2 summarises the transport coefficients for impurities in the various plasma conditions discussed in this section.

TABLE 2

Summary of impurity transport coefficients for the three types of the OS plasmas in JET

				Plasmas with Strong ITB	
		Radius (r/a)	**Plasma with Weak ITB (#38441)**	**L-mode edge (#40572)**	**ELMy edge (#40542)**
Nickel	**D (m^2/s)**	0 to 0.4 - 0.5	0.3 to 0.6	0.03 to 0.06	0.4 to 0.7
		0.6 to 0.9	6 to 8	0.6	4 to 6
		0.95 to 1.0	0.2 to 0.3	0.2	0.2 to 0.5
	V (m/s)	0 to 0.4 - 0.5	0 to -3	0	0 to -3
		0.6 to 0.7	-12	-6.5	-10
		0.75 to 0.9	-1 to -3	-1 to -2	-1 to -3
Carbon	**D (m^2/s)**	0.4 to 0.5	0.3	0.3	**(b)**
		0.6 to 1.0	2.5	0.3	
	V (m/s)	0 to 0.3	0 to 0.3	0 to -0.1	
		0.3 to 0.4	0.3 to 0.5	-4	
		0.5 to 1.0	-2 to -10	-0.5 to -3	

(a) the numbers quoted are given at approximated radial region. Please refer to Figures 8 – 13 for the central shape of the coefficients

(b) not available

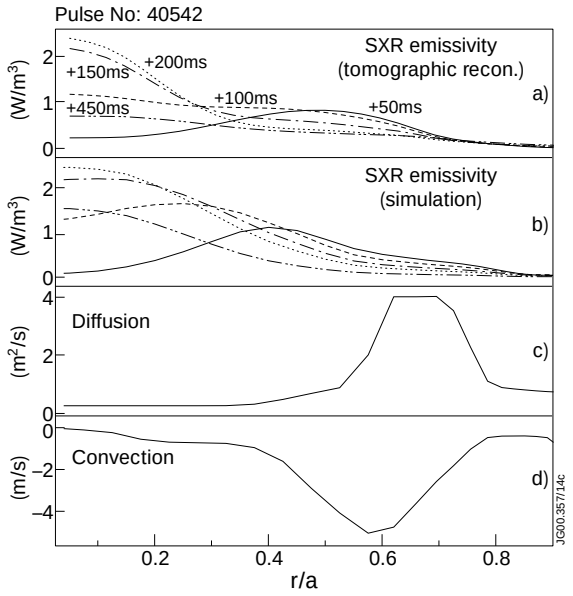

Figure 13: Nickel ion transport simulation in a strong ITB plasma with an ELMy edge (a) the time evolution of the flux surface averaged Soft X-Ray emissivity profiles from tomographic reconstruction (b) the computer simulated Soft X-Ray emissivity profiles for the same time slices (c) the diffusion coefficient profile and (d) the convection profile used in the simulation.

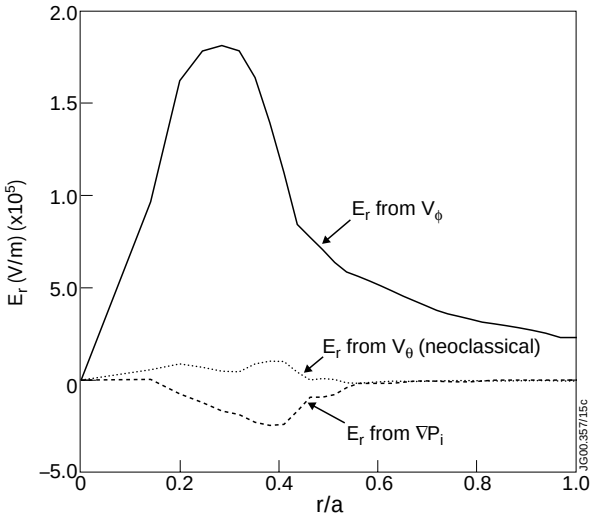

Figure 14: The contributions to from the three terms in the radial force balance equation calculated for C^{6+} using the FORCEBAL code for an OS plasma with strong ITB with L-mode edge (40572).

5. DISCUSSION

5.1 Neoclassical transport in JET OS plasmas

In JET OS plasma, diffusion inside a strong ITB is consistent with the neoclassical prediction. In the outer region the transport is anomalously high compared to the neoclassical prediction. Similar observations have been made in DIII-D. A strong Z dependence of the impurity profile has been observed in very high-mode (VH-mode) and negative central shear (NCS) plasmas [7] that is qualitatively consistent with neoclassical expectations. In other JET confinement scenarios, the departure of transport from the neoclassical level has also been observed to become larger towards the edge, such as in the ELMy H-mode [14, 29] and L-mode plasmas [8]. In L-mode plasmas, the diffusion coefficient was found to decrease in the plasma centre to D~0.2 m^2/s (still about 10 times higher than that predicted by neoclassical theory).

It was identified by Giannella [8] that the reduction of transport coincided with the location where magnetic shear equaled 0.5 for L-mode confinement. However in OS plasmas, the difference of transport does not seem to be solely connected to the magnetic shear. According to EFIT calculations, there is not much difference in the magnetic shear profiles for the strong and weak ITB plasmas. Therefore it is difficult to explain the large differences found in the ion transport by the profiles of the magnetic shear.

5.2 Convection and the transport barriers

The common feature of edge and internal transport barriers is the steepness of the local plasma temperature and density profiles. In a plasma with centrally peaked density and temperature profiles, the background ion density gradient drives an inward flux while the temperature gradient can drive an ion flux either inward or outward depending on which collisional regime the ions are in. This can be shown in a simplified formula from the neoclassical theory [30]:

where for the Pfirsch-Schlüter regime, $0.2 < H < 0.5$, and for the banana-plateau regime, $-1.5 < H < 0$. Subscript I stands for impurity and i for background ions. In the edge transport barrier region of H-mode plasmas impurities are in the Pfirsch-Schlüter collisional regime for a

$$V_I \propto Z\left(\frac{n_i'}{nD^{P-S}} - H\frac{T_i'}{T_i}\right)$$

typical edge density and temperature. The presence of main ion density gradient and temperature gradient could produce an inward convection, $V_I^{P-S} \propto Z_I(n_i'/n_i - 0.5T'/T)$, which is proportional to the ion charge. And experimentally an inward convection was found for H-mode edge [23, 31]. In the area of the internal transport barrier, impurities are mostly in the banana-plateau regime where a simple estimate of the convection is $V_I^{BP} \propto \sqrt{A_I}/Z_I(n_i'/n_i - 1.5T'/T)$, where $A_I = m_I/m_i$. We would therefore expect the convection to be inwards, driven by the gradients of main ion density and temperature gradients. Qualitatively, the neoclassical calculations of the convection velocities for Ni and C using FORCEBAL code show (Figure 9 and Figure 11) that both Ni and C have inward convection in the region of the ITB. In summary, a common feature of both H-mode and OS confinement is having an inward convection in the region of the transport barrier.

5.3 Influence of plasma rotation on transport

An extended neoclassical theory that includes the effect of toroidal plasma rotation, W, is being developed in order to account for the beam driven fast toroidal rotation in many tokamak experiments. The enhancement of the radial particle transport due to rotation was predicted for the Pfirsch-Schlüter regime [32, 33]. This modification could reduce to some extent the discrepancy between experimental and standard neoclassical theory discussed in the preceding sections. For the case of a trace impurity in the Pfirsch-Schlüter regime, an enhancement of impurity transport has been predicted for two ion species and with circular flux surfaces [32]:

$$D = D^{P-S}\left(1 + \frac{m^*\Omega^2 R_0^2}{2T_i}\right)^2$$

where $D_{D^{P-S}}$ is the neoclassical Pfirsch-Schlüter diffusion coefficient in actual plasma geometry $m^* = m_I - Zm_iT_e/(T_e + T_i)$. has a dimension of mass. Applying to nickel impurity in the Pfirsch-Schlüter collisional regime in the edge of JET high confinement plasmas, we found

that the enhanced diffusion is about 1.5 times higher than that from the neoclassical calculation using FORCEBAL. This is still too low compared with the experimental result.

5.4 Radial electric field in the region of internal transport barriers

It is straight-forward to calculate the radial electric field from the radial force balance, given the measured quantities such as plasma pressure gradients , plasma rotation velocities (v) in both toroidal and poloidal directions, and magnetic fields. Applying $E_r = (1/Z_I en_I)\nabla_r P_I + v_{\phi I} B_\theta - v_{\theta I} B_\phi$ we can derive the in JET plasmas for C^{6+} as all the variables in the right-hand-side are measured for C^{6+} ions except the poloidal rotation velocity, for which we use the neoclassical value. Figure 14 shows a calculation of the above equation for a plasma with a strong ITB, in which the contributions from each term are indicated.

An interesting fact is that in the calculations, the contribution for the E_r arises mainly from the toroidal plasma rotation, rather than from the poloidal rotation or from the plasma pressure gradients, as has been reported in experiments on other tokamak devices [5]. The results from JET could have important implications in the understanding and utilisation of the mechanism of the transport barriers: by externally driving the rotation of the plasma, the required shearing rate of could be produced to reduce the transport of the plasmas.

5.5 Velocity shear turbulence suppression

The mechanism of turbulence suppression is of great interest to fusion research, particularly in the H-mode edge barrier and OS internal transport barrier. It was shown that impurity ion transport reduces and is close to the neoclassical value towards the core of plasmas with respect to the edge region in ELMy H-mode [29] and with OS confinement, Section 4. It has been demonstrated using a simple model that the presence of the velocity shear results in de-correlation of turbulence [34]. The de-correlation of the density and velocity perturbations results in the decrease of radial transport.

Numerical models [35] show that velocity shear can also affect nonlinearly saturated turbulence. Because the flow is the same for all particles regardless of their charge or mass, it affects to all turbulent modes if the velocity shear is sufficiently large. A semi-empirical rule [36] states that the toroidal ion temperature gradient (ITG) mode turbulence will be greatly reduced or even completely quenched when the velocity shear rate is greater than the maximum linear growth rate of the ITG ballooning modes computed in the condition without the shear.

It has been reported that this rule agrees well with experimental results [37]. It is believed that a strong gradient in the profile can suppress the growth of certain turbulent modes, and the transport of plasma is hence reduced to collisional transport level. The shearing rate in a toroidal geometry is defined [38] as:

$$\omega_{E\times B} \cong \frac{RB_\theta}{B_\phi}\frac{\partial}{\partial r}\left(\frac{E_r}{RB_\theta}\right)$$

The calculation of was carried out using the FORCEBAL code for strong and weak ITB plasma. The radial derivative in this code is calculated with respect to the major radius on the outer mid-plane. The maximum linear growth rate of the ITG ballooning modes is about 1×10^5 s^{-1}.

Figure 15 shows the comparison of the in a strong and weak ITB plasmas. The in strong ITB plasma is well above the growth rate of the ITG modes, and is a factor of about 5 higher than in a weak ITB. This is a strong indication that the may be responsible for the reduced transport in plasma with a strong ITB, while in the weak ITB plasma, the is not large enough to suppress the turbulence.

5.6 ITG driven turbulent impurity transport models

Few numbers of articles have been devoted on the theoretical studies of turbulent driven impurity transport. Among them, some initial estimations of the heavy impurity diffusion coefficients arising from various classes of micro-instabilities has been studied by Wilson and Connor [39]. Here we discuss two turbulent transport models involving ion temperature gradient driven (ITG) mode against the experimental data. One model is the toroidal ITG model [40]. This model has been successful in the interpretation of ion thermal diffusivity. The ITG mode is driven by ion temperature gradient and is considered to be one of the major instabilities present in the bulk plasma. This model implies a Gyro-Bohm transport scaling since it gives a diffusion coefficient containing a factor $D_{GB} \sim \rho_s^2 c_s / R$ and it falls towards the plasma edge for the OS plasma with a strong ITB. The overall shape of the diffusion coefficient from this model does not fit the simulated diffusion coefficient, and the discrepancy increases towards the central region. Another model involving ion temperature gradients driven instabilities is based on the ITG driven trapped ion instability analysed by [41]. A preliminary agreement of this model to impurity transport in JET L mode plasmas has been pointed out by Connor [42] and by Lauro-Taroni [43]. The diffusion coefficient predicted by this model has a bell-like shape that results from the Gyro-Bohm like diffusion in the edge and its aspect-ratio dependence in the central region. Although the overall shape of the diffusion profile is close to the experimental simulation, in particular, the drop of diffusion position in the central region appear to be correlated with the ITB location, the peak diffusion value from the model is about one order of magnitude lower than experimental results. Therefore, both the toroidal ITG mode and the ITG driven trapped ion instability model are unlikely to be the transport mechanism in the OS plasma.

6. SUMMARY

JET optimised shear plasmas exhibit internal transport barriers indicated by the steep gradients in ion temperature and rotation profiles. The electron density profile is progressively peaked in the centre during OS confinement. Observations during impurity transport experiments show that, although in general there is no significant increase of Z_{eff}, carbon seems to follow the electron density profiles inside the internal transport barrier (ITB), and there is a slight increase of carbon ion density with time. Tomographic reconstruction of the Soft X-Ray emission

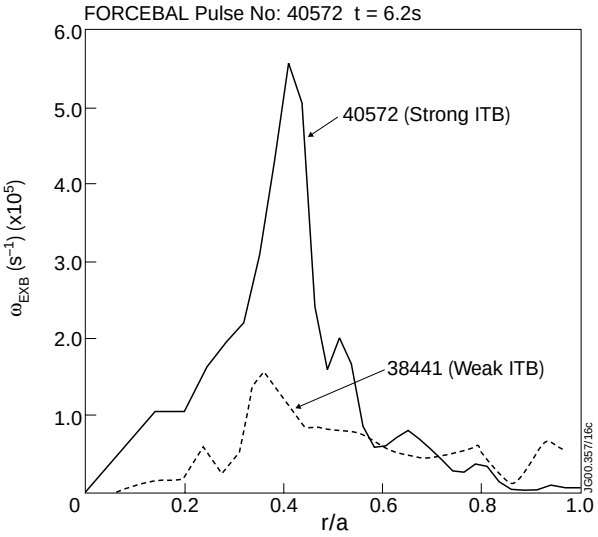

Figure 15: E×B shearing rate calculated for C^{6+} with the FORCEBAL code.

following the trace nickel injections shows that nickel ion transport is sensitive to the steepness of the ITB. A strong steep ITB prevents the nickel ions from getting into the plasma centre while rapid transport occurs in weak ITB plasmas. The behaviour of impurity ions is affected by the plasma edge condition. With an ELMy edge, there is no build up of impurities and therefore the combination of an ELMy edge with a strong ITB could be an attractive mode of operation for the OS plasma. An ELMy edge regime could be an attractive operation mode for the OS plasma [44].

By combining a strong ITB and an ELMy H mode edge, it is expected that the plasma will not suffer from the accumulation of some impurity species, while good core confinement is obtained. In fact, experiments have been carried out in JET to control edge conditions using radiating mantle by injecting impurities such as neon and argon [45, 46]. Time dependent local impurity diagnostics, such as soft X-ray cameras and charge exchange spectrometers enable local evaluation of the transport coefficients directly from the local variation of impurity density and flux.

The impurity transport model can be checked by the achieving consistency among different measurements and simulations. The main features of the impurity ion transport are summarised as follows:

1. In general, the impurity transport in the plasma core region is smaller than that in the edge area. In the central region, the impurity ion transport is dominated by diffusion. Detailed differences are distinguished in plasmas with different ITB strength and different edge conditions.
2. Inside a strong ITB, a greatly reduced diffusion transport coefficient to the level of the neoclassical prediction was found for the nickel ion transport, and it is about 10~50 times lower than the region outside the ITB. The region of the diffusion reduction extends from the barrier position to the axis. The reduction of the impurity transport is less pronounced in the central region of the plasmas with weak ITBs. In weak ITB cases, the diffusion coefficient is about 10 times larger than in the strong ITB cases.
3. ELMs in the plasma edge can cause a large difference in the global ion transport. In the central region of plasmas with strong ITBs, the nickel ion transport is higher (by 5~10 times) in the case of an ELMy H-mode edge than with L-mode edge.

4. An inward convection is present in the vicinity of a strong ITB.

In the core region of strong internal transport barriers, neoclassical transport could be the mechanism for the ion transport, and there is a quantitative agreement between experimental results and the theory. A departure from neoclassical theory is found in the outer region of the plasma. An inward convection of impurities is a feature common to both edge and internal transport barriers. Qualitatively, neoclassical theory can account for the presence of a convection velocity in the transport barrier region. Extended neoclassical theory, including the toroidal plasma rotation, gives an enhancement of the impurity ion transport and leads to a reduction in the discrepancy between the experimental value and neoclassical transport theory.

The correlation of impurity transport and the $E \times B$ shear rate shows that the difference in nickel transport between strong and weak ITB plasmas may be caused by the suppression of turbulence in the strong ITB area that results from a strong $E \times B$ shear rate. Toroidal ion rotation, from unbalanced NBI, appears to play a critical role in JET plasmas. Among the three components in the radial force balance, ∇P_i, $V_\theta B_\phi$ and $V_\phi B_\theta$, $V_\phi B_\theta$ is the dominant contributor to radial electric field. Also the radial gradient of $V_\phi B_\theta$ is the dominant contributor to the $E \times B$ shearing rate.

ACKNOWLEDGEMENTS

We would like to acknowledge the invaluable collaboration with JET Experimental Division managed by Dr Paul Thomas. In particular we are thankful for the very beneficial suggestions and assistance from Drs. Ruggero Giannella, Laura Lauro-Taroni, Manfred von Hellermann, Klaus-Dieter Zastrow, Ivor Coffey, Martin O'Mullane, Kerry Lawson, Robin Barnsley, Barry Alper, Richard Gill, Michele Romanelli and Vasili Parail. We thank the former JET Physics Task Force, in particular, Drs. Claude Gormezano and Franz Söldner for their collaboration on the impurity injection experiment during optimised shear confinement operation. Dr. Wayne Houlberg of Oak Ridge National Laboratory is acknowledged for his permission and help to use the FORCEBAL code. H. Chen also would like to acknowledge her joint funding by an Oversea Research Student (ORS) award and the UK Department of trade and industry and EURATOM. The completion of the paper was partly supported (H. Chen) under the auspices of the U.S. DOE by University of California Lawrence Livermore National Laboratory under contract No. W-7405-Eng-48.

REFERENCES

* Present address: Lawrence Livermore National Laboratory, Livermore, CA 94551, USA

[1] Levinton F M, et al., Phys. Rev. Lett. **75** (1995) 4417

[2] Strait E J, et al., Phys. Rev. Lett, **75** (1995) 4421

[3] The JET Team (presented by Gormezano C), 16th IAEA Fusion energy conference, IAEA-CN-64/A5-5, Canada, 1996

[4] Koide Y and JT-60U Team, Plasma Physics, **4** (1997) 1623

[5] Synakowski E J, Plasma Physics, Controlled Fusion. **40** (1998) 581

[6] Hirshman S P and Sigmar D J, Nuclear Fusion, **21** (1981) 1079

[7] Wade M R, Houlberg W A, and Baylor L R, "Evidence of neoclassical impurity transport in DIII-D", Transport Task Force meeting, Atlanta, USA,1998

[8] Giannella R , et al., Nuclear Fusion, **34** (1994) 1185

[9] Mattiolo M, et al, Nuclear Fusion, **35**, (1995)1115

[10] Dux R, Peeters AG, Gude A, et al, Nuclear Fusion **39**, (1999)1509

[11] http://epub.iaea.org/fusion/public/39/dec/Chapter2

[12] Magyar G, "The laser blow-off system (KZ3) on JET", JET report (1988)15

[13] Alper B et al., Rev Sci. Instument, **68** (1997) 778

[14] Ingesson L C , et al. Nuclear Fusion, **38** (1998) 1675

[15] Blackler K and Edwards A W, IEEE Transaction on Nuclear Science, **41** (1994) 111

[16] Mast K F, et al., Rev Sci Instrum **56** (1985) 969; Reichle R, et al., in Diagnostics for Experimental Thermonuclear fusion reactors, eds P E Stott, ESindoni, (New York,Plenum) (1996) 61

[17] Fonck R J, et al., Applied Optics, **21** (1982) 2115

[18] Bartiromo R, et al., Rev. Sci. Instrum. **60** (1989) 237; Barnsley R, et al., Rev Sci Instrum, **63** (1992) 5023

[19] von Hellermann M and Summers H, "Active Beam Spectroscopy at JET", Atomic and Plasma-Material Interaction Processes in Controlled Thermonuclear Fusion, R K Janev H W Drawin editors, Elsevier, (1993) 135

[20] Wade, M R, Whyte, D G, Wood, R D, West, W P, 23rd EPS conference, Kiev, (1996)

[21] Bell R E, et al. Plasma Physics, Controlled Fusion, **40** (1998) 609

[22] Behringer K H, Report, JET-R(1987)08

[23] Lauro-Taroni L, et al., Proc. 21st EPS conf. on Controlled Fusion and Plasma Physics, Montpellier, **I** (1994) 102

[24] Summers H P, "Atomic Data and Analysis Structure," JET Report IR (12) 1994

[25] Houlberg W A, Shaing K C, Hirshman S P and Zarnstorff M C, Plasma Physics, **4** (1997) 3230

[26] Lao L L, et al. Nuclear Fusion, **25** (1985) 1611

[27] Denne-Hinnov B, et al., Proc. 20th EPS conf. on Controlled Fusion and Plasma Physics, Lisboa, Vol. 17C, **I** (1993) 55

[28] Lawson K D, et al., "Impurity transport in JET L-mode discharges", submitted to Nuclear Fusion, (1999)

[29] Giannella R, et al., Proc. 24th EPS conf. on Controlled Fusion and Plasma Physics, Berchtesgarden, **I** (1997) 53

[30] Fussmann G , et al., J. Nuclear Materials **162-164** (1989) 14; Fussmann G, Nuclear Fusion, **26** (1986) 983

[31] Hawkes N C, et al., Proc. 16th EPS conference on Controlled Fusion and Plasma Physics, Geneva, **I** (1989) 79

[32] Romanelli M, Chen H, LC Ingesson, L Lauro-Taroni, M Ottaviani, Proc. 25th EPS conf. on Controlled Fusion and Plasma Physics, Prague, (1998)

[33] Helander P, Plasma Physics, **5**, (1998) 3999

[34] Burrell K H , Plasma Physics, **4** (1997) 1499

[35] Waltz R E, Kerbel G D, Milovich J, Plasma Physics, **1** (1994) 2229; Carreras B A, et al., Physics Fluids, B, **4** (1992) 3115

[36] Waltz R E, Dewar R L, Garbet X, Plasma Physics, **5** (1998) 1784

[37] Carreras B A, IEEE Transactions on Plasma Science **25** (1997) 1281

[38] Hahm T S and Burrell K H Plasma Physics, **2** (1995) 1648

[39] Wilson H R and Connor J W, "Theories of anomalous impurity transport", *Internal report*, Culham Laboratory 1993

[40] Romanelli F and Zonca F, Phys. Fluids B, **5**, (1993)4081

[41] Biglari H, Diamond P H and Rosenbluth M N, Fluid Physics, B, **1**, (1989)109,

[42] Connor J W, Plasma Phys. Control. Fusion, **37**, (1995) A119,

[43] Lauro-Taroni L, et al., 22nd EPS conf. on Controlled Fusion and Plasma Physics, Bournemouth, 1995

[44] Söldner F X, et al., Nuclear Fusion, **39** (1999) 1883

[45] Zastrow K-D, et al., 26th EPS conference, Maastricht, (1999)

[46] Nave MFF, et al., 26th EPS conference, Maastricht, (1999)